Suspensions of Silica Particles Grafted with Concentrated Polymer Brush: Effects of Graft Chain Length on Brush Layer Thickness and Colloidal Crystallization

Kohji Ohno, Takashi Morinaga, Satoshi Takeno, Yoshinobu Tsujii, and Takeshi Fukuda*

Institute for Chemical Research, Kyoto University, Uji, Kyoto 611-0011, Japan

Received August 6, 2007; Revised Manuscript Received October 9, 2007

ABSTRACT: We previously reported that monodisperse silica particles (SiPs) afforded with a high-density brush of poly(methyl methacrylate) (PMMA) and suspended in a good solvent for PMMA formed a colloidal crystal in a certain concentration range (*Macromolecules* **2006**, *39*, 1245). Here we investigated similar hybrid particles with respect to the influence of graft chain length L_c on their hydrodynamic diameter D_h in dilute suspension and on colloidal crystallization in more concentrated suspension. The average radius r_0 of SiPs was 65 nm, and the surface density σ_0 of PMMA grafts at the SiP surface was about 0.7 chains/nm^2 (about 36 000 chains per particle). The hydrodynamic thickness of the swollen brush layer h ($=D_h/2 - r_0$) was qualitatively interpretable by a modified Daoud−Cotton-type scaling model. Namely, for short graft chains, h obeyed the universal relation, $h[1 + (h/2r_0)] \sim L_c\sigma_0^{1/2}$, applicable to *concentrated polymer brushes* on flat as well as spherical surfaces, and for chains longer than a critical length, h showed positive deviations from this linear relation, indicating the brush layer getting into the *semidilute polymer brush* regime. Suspensions of the hybrid particles showed a phase transition from a (disordered) fluid to a fully crystallized system with a narrow fluid/crystal coexisting regime. The critical concentration of crystallization (melting point) decreased with increasing graft chain length, and the nearest-neighbor interparticle distance D_{dis} in the crystal approached to a micrometer scale as the graft molecular weight reached 500 000. Good correlation was observed between D_h and D_{dis} such that $D_{dis} = (1.15 \pm 0.05)D_h$. Confocal laser scanning microscopic observation suggested that the colloidal crystal generally include both hexagonal close-packed (hcp) and face-centered cubic (fcc) lattice arrangements with the fcc arrangement likely to increase with increasing chain length.

Introduction

Colloidal crystals have attracted much attention for fundamental understanding of condensed matter crystallization[1−13] as well as for their potential applications, in particular, as photonic crystals which are characterized by alternating domains of higher and lower refractive indices with a periodicity on the order of the wavelengths of visible lights.[14−16] Typical colloidal crystals are formed by spherical particles suspended in a liquid. Driving forces for the formation of colloidal crystals are believed to be repulsive potentials working between colloidal particles, of which typically two types are known. One is the hard-sphere potential, which is steric and short-range in nature, inducing crystallization of rigid uncharged particles (*hard* colloidal crystal).[3−6,9,10] The other is the electrostatic potential, which can be of extremely long range depending on the ionic strength of the system, inducing crystallization of charged particles (*soft* colloidal crystal).[7,8,17,18]

Recently, we have identified a colloidal crystal for a suspension of hybrid particles having a spherical silica core and a shell of well-defined poly(methyl methacrylate) (PMMA) chains densely grafted on the silica surface.[19] This system is new and distinguished from any of previously observed colloidal crystals or similar ordered assemblies formed by polymers of special architecture such as block copolymers and star-shaped polymers. As a matter of fact, colloidal crystals of spherical particles with polymer chains terminally grafted on the surface have been known since the early 1970s, and it has been speculated that those graft chains would work as a repulsive interparticle potential barrier, a rather "soft" potential qualitatively analogous to the electrostatic one. However, in all of the previously studied systems of this kind,[3,4,6,9,10,12] the graft density was so low, and in many cases, the graft chain length was so small that the graft chains simply played the role of stabilizing the particles dispersed in a liquid and had no significant effect on the interparticle potential. Namely, all of them showed the characteristics of hard colloidal crystals, and the speculated effect of graft chains on interparticle potential had never been clearly demonstrated experimentally before the mentioned work by us.[19]

Particles with a densely grafted surface are expected to show qualitatively different properties from those with a moderately or sparsely grafted surface. To see this, a brief introduction to "polymer brushes (PB)" may be due:[20,21] Analogous to the notions of dilute, semidilute, and concentrated solutions of free chains, the assemblies of polymer chains end-grafted on a solid surface and swollen in a good solvent can be categorized into three regimes according to graft density (and chain length). When graft density is so low that the grafted chains do not overlap each other, the system is in the "dilute brush" regime, where the chains take the conformation of "mushroom" (a swollen coil somewhat deformed by the influence of the surface). When graft density exceeds a threshold value or region, the chains will overlap each other, and in order to avoid mutual interference, they will get stretched away from the surface. Such a system is termed a "semidilute polymer brush (SDPB)", in which the intermolecular segmental interactions are important, but both the volume fraction and deformation free energy of chains are still low enough that they can be approximated by the "binary segmental interaction" and the "Gaussian elastic free energy", respectively. As graft density further increases, the

* To whom correspondence should be addressed. E-mail fukuda@scl.kyoto-u.ac.jp.

10.1021/ma071770z CCC: $37.00
Published on Web 11/16/2007

system will ultimately get into the "concentrated polymer brush (CPB)" regime, where higher-order segmental interactions and the non-Gaussian nature of stretched chains become important. Theoretical studies have been carried out at varying levels of approximations for SDPBs (and CPBs, in some cases) on both flat[22−25] and curved[26−29] surfaces. On the other hand, experimental studies had been virtually limited to SDPBs because of the unavailability of CPB samples until recently, when living radical polymerization (LRP) proved to be capable of routinely providing well-defined polymer brushes with graft densities up to 0.3−0.5 in surface coverage.[20,21] These graft densities are more than 1 order of magnitude higher than those of typical SDPBs, going deep into the CPB regime. Systematic experimental studies of CPBs got started then, disclosing many unique properties of them, such as unusually high glass transition temperature,[30] high plate compressibility in swollen[31,32] and dry[33] states, sharp size-exclusion effects by swollen[34] and dry[21] CPB layers, extremely large thickness of swollen CPBs,[31,32] and pressure-independent ultrahigh lubricity of confronted swollen CPBs.[21]

The last two properties of CPBs are particularly interesting with regard to the present work. The extremely large thicknesses of swollen CPBs, almost comparable to fully stretched chain lengths, would suggest an interparticle potential of that long range and its controllability by controlling chain length (and graft density). The mentioned ultrahigh lubricity of confronted CPBs comes from the *non-interpenetrating* or *demixing* interaction between them, originating from the highly extended chain conformation of CPB chains. This suggests a hard-sphere-type potential between CPB-afforded particles. Of course, the effective surface density of the brush is not constant but varies with varying radial distance from the sphere center. Accordingly, not only the mean thickness of the brush layer but also the radial concentration profile of polymer segments and hence the interparticle potential should be functions of the surface density and chain length of graft polymer as well as the size of the core particle. These important and interesting features of CPB-afforded particles and their colloidal crystallization had never been studied previously, and this has motivated us to conduct a series of systematic experimental studies to elucidate details.

In the previous paper,[19] we have demonstrated the colloidal crystallization of the hybrid particles with a particular silica core (diameter 130 nm) and a particular PMMA CPB (graft density about 0.7 chains/nm^2 and graft chain molecular weight about 180 000). A very long range of interparticle potential afforded by the graft chains was suggested by the low particle concentration at colloidal crystallization and the large size of the crystalline unit lattice. In this work, we will study similar hybrid particles of varying PMMA chain lengths with the same core diameter and nearly the same (high) graft density as in the previous work. By changing the graft chain length from short to long ones, the effective surface density will go from CPB to SDPB regimes. The central aim of this work is at quantitatively studying the chain length dependence of the mean thickness of brush layer and the critical concentration of colloidal crystallization and elucidating possible correlation between them. Another important and interesting problem of possible chain length dependence of colloidal crystalline structure will also be studied by the in situ observation of crystals on a confocal laser scanning microscope.

Experimental Section

Materials. SiP (SEAHOSTER KE-E10, 20 wt % suspension of SiP in ethylene glycol) was kindly donated by Nippon Shokubai Co., Ltd., Osaka, Japan. The mean diameter of the SiP was 130 nm with a relative standard deviation of 10%, as measured by transmission electron microscopy. The hybrid particles (PMMA−SiPs) were synthesized by surface-initiated atom transfer radical polymerization (ATRP)[35] of MMA, as reported previously.[36] The characteristics of PMMA−SiPs used in this work are summarized in Table 1. Chloroform (99.5%), 1,2-dichloroethane (99.5%), cholorobenzene (99%), and *o*-dichlorobenzene (99%) were used as received from Nacalai Tesque Inc., Osaka, Japan.

Table 1. Characteristics of Silica Particles Grafted with Concentrated PMMA Brush[a]

sample code	M_w[b]	M_w/M_n[c]	graft density (chains/nm^2)	D_h[d] (nm)	d_s[e] (%)
P1	88 000	1.28	0.59	300	5.3
P2	126 000	1.24	0.62	350	5.2
P3	188 000	1.19	0.73	450	5.1
P4	293 000	1.27	0.71	580	4.5
P5	518 000	1.20	0.71	840	4.9
V1	126 000	1.36	0.59	350[f]	

[a] The diameter of the silica particle core was 130 nm. [b] Weight-average molecular weight of PMMA grafts. [c] Polydispersity index (PDI) of PMMA grafts. [d] Average hydrodynamic diameter determined by dynamic light scattering in acetone at 30 °C, except for sample V1. [e] Relative standard deviation determined by dynamic light scattering. [f] Estimated from the intrinsic viscosity $[\eta]$ determined in tetrahydrofuran at 30 °C, according to $[\eta] = (5\pi N_A D_h^3)/(12M)$, where N_A is the Avogadro's number, and M is the mass per hybrid particle. Since the size distribution of the hybrid particles is generally small (cf. the values of d_s given in this table), and since the difference of the two (good) solvents should have no important effect on the swollen thickness of *concentrated* brushes (see text), this viscosity data for sample V1 may reasonably be compared to the DLS data for sample *P*2.

Preparation of PMMA—SiP Suspensions for Colloidal Crystal Formation. The PMMA−SiP hybrid particles were dispersed in mixed solvents matching both their refractive index n and density ρ. Sample P1 (see Table 1) was dispersed in a mixture of 1,2-dichloroethane/chloroform/*o*-dichlorobenzene of volume composition 76/1/23. The n and ρ of this solvent mixture, approximated by composition-averages of those of the pure solvents, were 1.47 and 1.27 g/cm^3, respectively, and approximately equal to those of P1. Similarly, samples P3 and P5 were dispersed in mixtures of 1,2-dichloroethane/chlorobenzene/*o*-dichlorobenzene of 53/20/27 (approximate n and ρ: 1.49 and 1.24 g/cm^3) and 31/69/0 (approximate n and ρ: 1.50 and 1.15 g/cm^3), respectively. The refractive index matching provides nearly transparent suspensions, which is essential for optical observations, and the density matching reduces the effect of gravity, which is essential for the system to achieve a thermodynamic equilibrium.[2−5]

Dynamic Light Scattering. Dynamic light scattering (DLS) measurements were made in acetone solvent at 30 °C on a DLS-7000 photometer (Otsuka Electronics, Japan) with a He−Ne laser (wavelength 633 nm and power 10 mW) as a light source. The scattering light intensity was measured at a scattering angle of 90°. The intensity correlation function $g^{(2)}(\tau)$ can be given by a single-exponential function, as follows,

$$g^{(2)}(\tau) = 1 + \exp(-2\Gamma\tau) \quad (1)$$

where Γ is the characteristic rate for the translational diffusion and τ is the correlation time. Γ is related to the translational diffusion coefficient D_{dif} by

$$\Gamma = D_{dif}q^2 \quad (2)$$

where q is the scattering vector. The hydrodynamic diameter D_h can be calculated by the Stokes−Einstein equation

$$D_h = k_B T/3\pi\eta D_{dif} \quad (3)$$

where η is the solvent viscosity, k_B is the Boltzmann constant, and T is the absolute temperature.

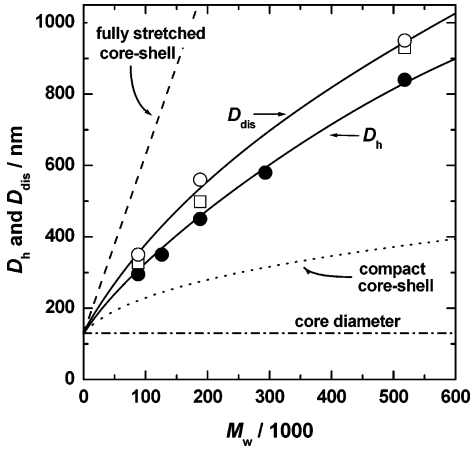

Figure 1. Plot of average hydrodynamic diameter D_h of silica particle densely grafted with poly(methyl methacrylate) (PMMA−SiP) as a function of weight-average molecular weight M_w of the PMMA graft chains. The D_h values were determined by dynamic light scattering in dilute acetone suspension at 30 °C. The diameter of SiP core is 130 nm. The broken and dotted lines represent the diameters of the fully stretched and compact core−shell models, respectively (see text).[19,37] The open circles show the nearest-neighbor center-to-center distance D_{dis} between particles at the melting concentration of the crystal, as observed by confocal laser scanning microscopy (CLSM: see Figure 7), and the open squares show values of s_cD_h, where s_c is the space parameter of hard crystals ($s_c = 1.11$; see text).

Confocal Laser Scanning Microscopy (CLSM). CLSM observation of the colloidal crystals was made on an inverted type microscope (LSM 5 PASCAL, Carl Zeiss, Germany) with a 458 nm wavelength Ar laser and 63× objective (Plan Apochromat, Carl Zeiss) in reflection mode. Other experimental details were as described previously.[19]

Results and Discussion

Hydrodynamic Thickness of Brush Layer: Experimental Results. DLS measurements were conducted for a series of hybrid particles with a fixed diameter of silica core of 130 nm, nearly the same graft density, and various chain lengths of PMMA grafts. The characteristics of the hybrid particles including their hydrodynamic diameters D_h and standard deviations d_s determined by DLS are given in Table 1. The intrinsic viscosity measurement made for one PMMA−SiP sample (sample V1) having nearly the same characteristics as sample P2 gave a D_h value consistent to that of P2 determined by DLS (see Table 1). Figure 1 shows the plot of D_h as a function of weight-average molecular weight M_w of the PMMA grafts. The diameters of the compact core−shell model[19,37] and the fully stretched core−shell model[19,37] are also shown in the figure. The former model consists of a SiP core and a PMMA shell of bulk density, and the latter one consists of a SiP core and a PMMA shell whose size is equal to that of the PMMA chains radially stretched in all-trans conformation. The D_h value increases with increasing M_w, being intermediate between the diameters of the two models. The hydrodynamic thickness h of the brush layer may be calculated by the equation $h = (D_h - D_0)/2$, where D_0 is the diameter of the SiP core (130 nm). The values of h are generally very large compared to the dimensions of the (free) graft chains. The double logarithmic plot of h vs M_w (not shown) gave an approximately linear relation, showing that h was proportional to M_w^b with $b = 0.83$.

Theoretical Analysis of Brush Layer Thickness. In order to understand the observed values of h and the exponent b, we will consider the scaling-theoretical model due to Daoud and Cotton[26] (DC) by somewhat modifying it. The numerical coefficients of the scaling results[26,27] have been elaborated by more recent and elegant treatments.[28,29] However, our concern here is not to discuss the numerical terms but, as suggested in Introduction, to address the brush regimes and estimate the concentrated to semidilute (CPB to SDPB) crossover chain length by the aid of theory. For this purpose, the simple scaling treatment giving analytical results will be useful and sufficient. The notion of CPB and SDPB itself comes from the scaling-theoretical picture, as noted in Introduction. The more recent treatments[28,29] pay little attention to this notion or, more precisely, to the region of CPB.

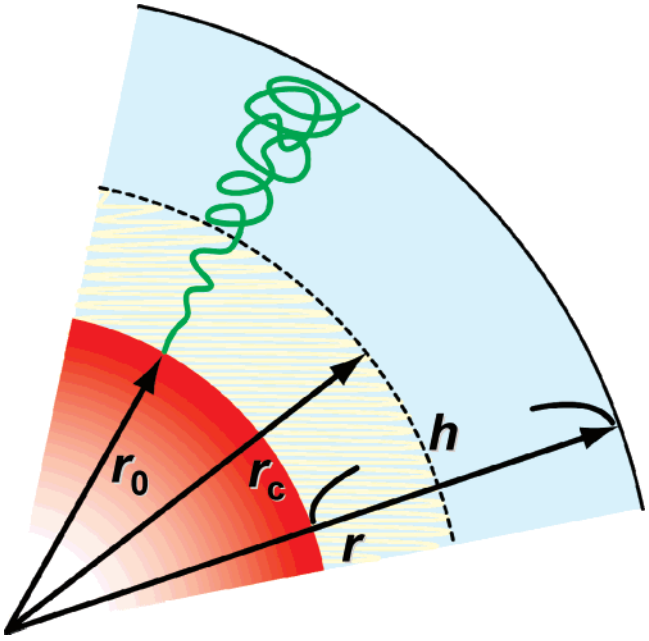

Figure 2. Schematic representation of the radius r_0 of core particle, the radius r of hybrid particle, the thickness h of brush layer, and the concentrated-to-semidilute (CPB-to-SDPB) crossover radius r_c.

The DC model is for symmetrical star-shaped chains, consisting, in our terms, of a spherical core of radius r_0 (=$D_0/2$), from which f graft chains of the same length are radially extended out. The effective graft density σ_{eff} decreases with increasing radial distance according to $\sigma_{eff} = \sigma_0(r_0/r)^2$, where σ_0 is the graft density on the core surface in unit of chains/nm^2, and r is the distance from the core center (Figure 2). When σ_{eff} is large enough, we are in the CPB regime, where the excluded-volume effect is screened out (the chain expansion factor $\alpha = 1$). As r increases beyond the crossover radius r_c, we get into the SDPB regime, where r_c is given by

$$r_c = r_0\sigma_0^{*1/2}\upsilon^{*-1} \tag{4}$$

In eq 4, $\upsilon^* = (4\pi)^{1/2}\upsilon$, where υ is the excluded-volume parameter as defined by DC,[26] and σ_0^* is the dimensionless graft density (surface coverage) given by $\sigma_0^* = \sigma_0 s_m$, where s_m is the cross-sectional area of graft chain. The DC model with its core of star chains reinterpreted as *a foreign spherical particle of arbitrary size including no star-chain moiety* and σ_0^* being approximated by $\sigma_0^* = fl_m^2/4\pi r_0^2$, where l_m is the chain contour length per monomer unit, leads to the following expressions for the thickness h of the brush layer on the particle for three different cases.

Case 1: $r_0 < r_c$ and $r < r_c$. The whole brush layer is in the CPB regime, where we have

$$h[1 + (h/2r_0)] = aL_c\sigma_0^{*1/2} \tag{5}$$

In eq 5, a is a proportionality constant of order of unity (vide infra), and L_c is the full length of graft chain, $L_c = Nl_m$ with N being the degree of polymerization. Equations 4 and 5 along with the condition $r = r_0 + h < r_c$ give the criterion for the concentrated brush regime in terms of chain length:

$$L_c < (r_0/2a\sigma_0^{*1/2})(\sigma_0^*\upsilon^{*-2} - 1) \quad (6)$$

For the special case in which $h/r_0 = 0$ (flat surface), eq 5 reduces to[19,26]

$$h = aL_c\sigma_0^{*1/2} \quad (7)$$

Thus, the model predicts that the "universal" plot of $h[1 + (h/2r_0)]$ against $L_c\sigma_0^{*1/2}$ will give a straight line for any chain length, graft density, and surface curvature, insofar as the system is in the CPB regime. (We incidentally note that a simple extension of the model to CPBs on a cylinder of radius r_0 gives

$$(2r_0/3)\{[(1 + (h/r_0)]^{3/2} - 1\} = aL_c\sigma_0^{*1/2} \text{ (cylinder)}$$

which, for small values of h/r_0, can be cast into the same form as eq 5 with its $h/2r_0$ term on the left-hand side replaced by $h/4r_0$.)

Case 2: $r_0 \geq r_c$. The whole brush layer is in the SDPB regime, where we have

$$(h + r_0)^{5/3} - r_0^{5/3} = A \quad (8)$$

with

$$A = (5/3)aL_c r_0^{2/3}\sigma_0^{*1/3}\upsilon^{*1/3} \quad (9)$$

For the special case in which $h/r_0 = 0$ (flat surface), we recover the classic relation[22,23,27]

$$h = aL_c\sigma_0^{*1/3}\upsilon^{*1/3} \quad (10)$$

Case 3: $r_0 < r_c < r$. The brush layer has a CPB-to-SDPB crossover for $L_c \geq (r_0/2a\sigma_0^{*1/2})(\sigma_0^*\upsilon^{*-2} - 1)$ (cf. eq 6), where we have

$$(h + r_0)^{5/3} = A[1 + (5 + \sigma_0^*\upsilon^{*-2})(r_0/10aL_c\sigma_0^{*1/2})] \quad (11)$$

Since the systems that we experimentally study here should be related to either case 1 or case 3, we attempted to fit our data to eq 5 or 11 with a and υ^* as adjustable parameters. Figure 3 shows the double logarithmic plot of $h[1 + (h/2r_0)]$ vs $L_{c,w}\sigma_0^{*1/2}$, according to eq 5, where the subscript "w" attached to L_c denotes the weight-average[31] contour length of the chain. The solid curve in the figure demonstrates eq 5 calculated with $a = 1.15$, which fits the data points for the smallest three samples but shows deviations from those for the largest two samples. The broken curve shows eq 11 with $a = 1.15$ and $\upsilon^* = 0.3$, which can explain the deviations, suggesting that the deviations may originate in the excluded-volume effect.

This result suggests that the excluded-volume effect on h is insignificant for σ^*_{eff} larger than about 0.03. In fact, this σ^*_{eff} value corresponds to a "blob" size of about 5 nm or a PMMA molecular weight of about 10 000, for which the excluded-volume effect should be insignificant, and the relevant system may be considered to be in the CPB regime. This criterion of CPB (that σ^*_{eff} be larger than about 0.03) seems to be consistent with the published experimental data for a flat surface.[20,32] In Figure 4, two types of experimental data which meet this criterion of CPB are collected and plotted according to eq 5.

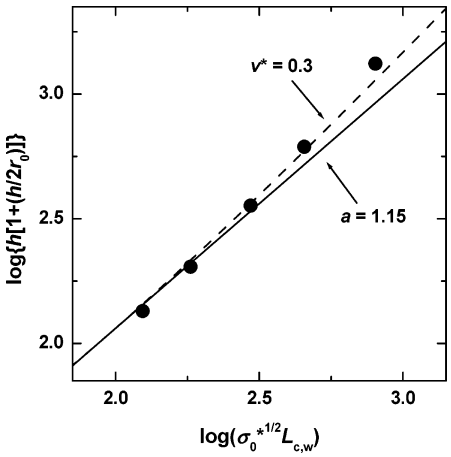

Figure 3. Double logarithmic plot of $h[1 + (h/2r_0)]$ against $L_{c,w}\sigma_0^{*1/2}$, where $L_{c,w}$ is the weight-average contour length (full length) of the graft chain, and σ_0^* is the dimensionless graft density (surface occupancy) of the brush on the core surface, $\sigma_0^* = s_m f/4\pi r_0^2$ with f being the number of graft chains per particle. The circles are experimental data for PMMA−SiP hybrid particles (data from Figure 1). The cross-sectional area s_m of PMMA unit was estimated to be 0.54 nm^2 by using the partial specific volume data[45] and the chain contour length, l_m, per monomer unit of 0.25 nm. The solid straight line shows the theory for concentrated polymer brushes (CPBs) (eq 5 with $a = 1.15$), and the dotted curve is the one for brushes with a CPB-to-SDPB crossover (eq 11 with $a = 1.15$ and $\upsilon^* = 0.3$; see text). For other symbols, see Figure 2.

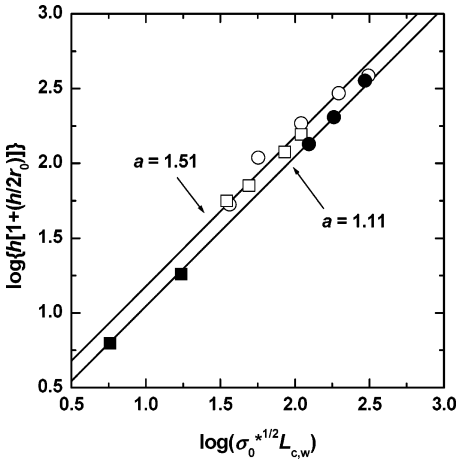

Figure 4. Double logarithmic plot of $h[1 + (h/2r_0)]$ against $L_{c,w}\sigma_0^{*1/2}$. The solid straight lines show the theory for CPBs (eq 5 with $a = 1.11$ and 1.51): (●) PMMA−SiP hybrid particles (this work); (■) PS−SiP hybrid particles (ref 38); (○) PMMA CPBs on a flat surface (ref 31); (□) PMMA CPBs on a flat surface (ref 32). Note that $h/r_0 = 0$ for flat surfaces. The cross-sectional area s_m of PS chain was estimated to be 0.62 nm^2 by using the partial specific volume data[45] (for other details, see Figure 2 and caption for Figure 3).

One type of data are for brushes on a spherical surface (Savin et al.[38] and this work), and the other type are for brushes on a flat ($h/r_0 = 0$) surface (Yamamoto et al.[31,32]). As eq 5 demands, both types of data are well represented by straight lines of unit slope with $a = 1.11$ (particle surface) and 1.51 (flat surface). The difference in a is attributed to the difference in the experimental methods to estimate h. The hybrid particle h was commonly estimated by DLS, which gives the hydrodynamic thickness of the brush, while the flat-surface h was estimated by atomic force microscopy (AFM), which is believed to give the equilibrium thickness of the brush layer. The mentioned result suggests that the AFM equilibrium thickness is significantly (some 30%) larger than the DLS hydrodynamic thickness.

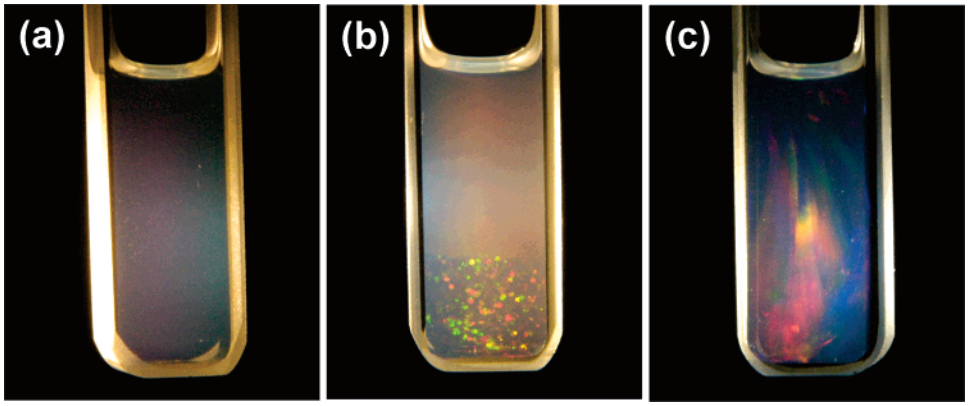

Figure 5. Photographs of suspensions of PMMA−SiP hybrid sample P5 (cf. Table 1) in the mixed solvent (1,2-dichloroethane/chlorobenzene = 31/69 volume ratio) illuminated from behind by white light; 2 weeks after sample preparation. The PMMA−SiP volume fractions (ϕ) were (a) 0.0375, (b) 0.0405, and (c) 0.0511. In sample a, the suspension remained slightly turbid without causing particle sedimentation. In sample b, crystalline and (random) fluid phases coexist. In sample c, strip-shaped colors gradually developed epitaxially from the top to the bottom of the suspension.

Table 2. Freezing and Melting Volume Fractions of PMMA−SiP Hybrid Particles Suspended in Isorefractive and Isobuoyant Mixture of Solvents[a]

sample	ϕ_f[b]	ϕ_m[c]	$(\phi_m - \phi_f)/\phi_f$
P1	0.129	0.136	0.054
P3	0.0795	0.0865	0.088
P5	0.0392	0.0425	0.084
ideal hard-sphere[d]	0.494	0.545	0.103

[a] For mixed solvents, see text. [b] Freezing volume fraction. [c] Melting volume fraction. [d] See ref 39.

Colloidal Crystallization. We previously reported that a PMMA−SiP hybrid system (sample P3 in Table 2) formed a colloidal crystal.[19] Another two samples P1 and P5 were studied here to see the effect of graft chain length on crystallization. PMMA−SiP suspensions in the solvent mixture with differing sample concentrations were placed in Pyrex glass cells (10 × 10 × 40 mm) connected with a glass tube, sealed off at the glass tube and allowed to stand at 25 °C for 2 weeks. Parts a−c of Figure 5 show the photographs of typical suspensions (sample P5) after 2 weeks, illuminated from behind by white light. The results were essentially similar to those previously observed for P3. Namely, suspensions with a relatively low particle concentration were an isotropic fluid, slightly turbid (due to the Tyndall scattering) without causing particle sedimentation, as shown in Figure 5a. On increasing particle concentration beyond a critical concentration, tiny iridescent flecks were observed soon after the onset of experiment, indicating the formation of Bragg-reflecting crystallites. As time elapsed, the formed crystallites sedimented very gradually under the effect of gravity, and the boundary between the iridescent-colored sediment (crystallites) and the slightly turbid supernatant (fluid phase) became more and more distinct, ultimately giving a sharp horizontal line, as shown in Figure 5b. This phase separation may be interpreted as a Kirkwood−Alder transition.[39,40] The sedimentation of the crystalline phase occurred because the average density of the hybrid particle was set slightly larger than that of the solvent (see Experimental Section), so that the density of the crystalline phase was slightly larger than that of the fluid phase.[4,6,19] As the particle concentration was increased, the volume percentage of the crystalline phase increased, and above another critical concentration, the entire body of the suspension was filled with crystallites. On further increasing the particle concentration, the suspension exhibited heterogeneously iridescent colors, of which three types were observed. In the first type, strip-shaped colors gradually developed epitaxially from top to bottom of the sample, as shown in Figure 5c. In the second type, needlelike crystallites were formed in part of the suspension. In the third type, heterogeneous iridescence appeared soon after the sample setting, which hardly changed throughout the experiment. These processes of coloring or structure formation are believed to depend essentially on particle concentration. More systematic investigation is needed to understand the phenomena observed

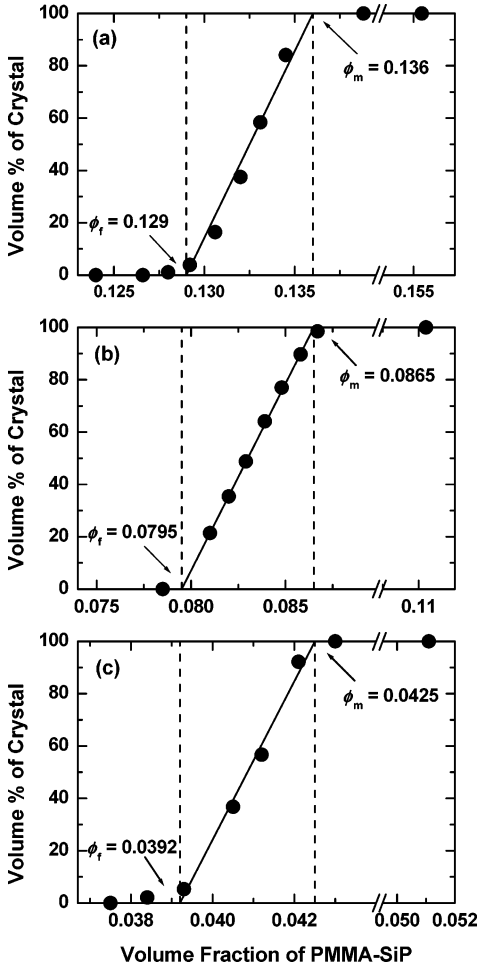

Figure 6. Phase diagrams showing the volume fraction of crystalline phase as a function of the volume fraction of PMMA−SiP hybrid particles P1, P3, and P5 suspended in the mixed solvents (see caption for Figure 5 and Table 1). Parts a, b, and c show the data for samples P1, P3, and P5, respectively.

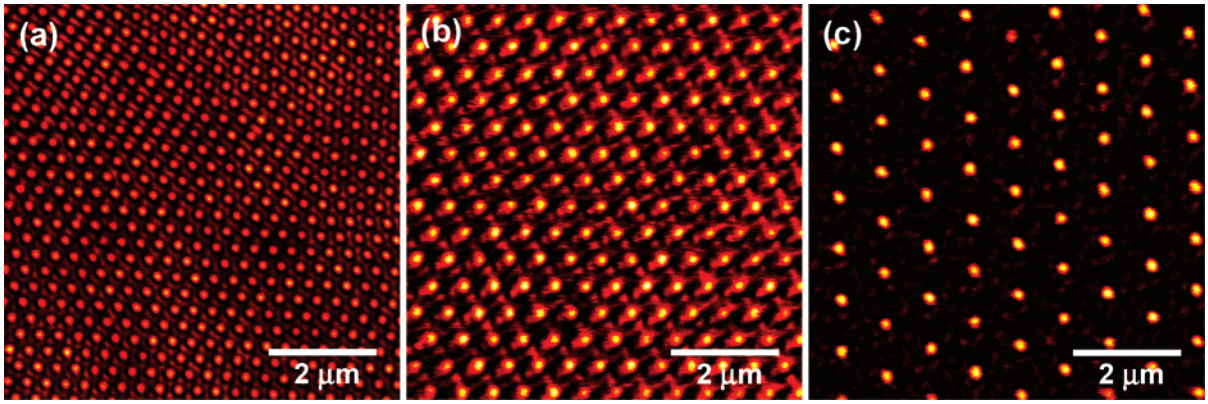

Figure 7. CLSM images of the (001) planes of the crystals formed by suspensions of silica particles (SiPs) densely grafted with poly(methyl methacrylate) (PMMA). Observations were performed using an Ar laser of 458 nm wavelength and a 63× objective in reflection mode. The distance of the focal plane from the inside of the coverslip was 50 μm. Parts a, b, and c show the data for PMMA−SiP samples P1, P3, and P5 (see Table 1), respectively. The mean nearest-neighbor center-to-center distances in the images a, b, and c are 350, 560, and 950 nm, respectively (see Figure 1).

at those relatively high particle concentrations, which is beyond the scope of the present work.

Phase Diagram. Figure 6 shows the phase diagrams of the suspensions of samples P1, P3, and P5, in which the volume percentage of the crystalline phase is plotted as a function of the volume fraction ϕ of the PMMA−SiP particle. In all cases, the plot shows a linear relationship in the fluid-crystal coexistence region, as is demanded for the coexisting two phases to be in a thermodynamic equilibrium. Extrapolation of the linear line to 0% and 100% crystal gives the freezing and melting volume fractions, ϕ_f and ϕ_m, respectively. The results are summarized in Table 2. The melting point ϕ_m decreased from about 0.14 for the smallest sample (P1) to about 0.04 for the largest sample (P5). Note again that ϕ is the sum of the volume fractions of the SiP core and grafted chains, and thus these results suggest that the values of ϕ_m of the present systems (spherical particles afforded with CPB) can possibly cover the volume fraction range throughout from typical soft ($\phi_m \sim 0.01$) to hard ($\phi_m = 0.545$) systems by simply changing the graft chain length. The relative width of the coexisting regime, $(\phi_m - \phi_f)/\phi_f$, is somewhat smaller than the computer-simulated value[39] of 0.103 for the hard crystal that is characterized by an ideal hard-sphere interparticle potential (see Table 2), presumably reflecting the difference in the potential curve.

CLSM Observation. The crystalline phase of each sample was in situ observed by CLSM. Figure 7 shows the CLSM images of the two-dimensional hexagonal close-packed (2D hcp) planes or (001) planes of the sample at the melting concentration. In all images, the SiP cores of the hybrid particles are clearly visible as yellow circles forming a 2D hexagonal array, while the PMMA brushes which should surround the SiP cores are hardly visible because of their much lower reflectivity. The high degree of positional order of the SiP cores and the strong dependence of the interparticle distance on the chain length of PMMA grafts are particularly noteworthy. The mean nearest-neighbor center-to-center distance D_{dis} in the images a−c in Figure 7 were measured to be 350, 560, and 950 nm, respectively. The distance D_{dis} can also be estimated from the melting concentration ϕ_m of the crystals, according to the following relation valid for closed-packed-type structures

$$D_{dis,cal} = 2^{1/6}(V_p/\phi_m)^{1/3} \tag{12}$$

where V_p is the particle volume of PMMA−SiP particle in unit of nm^3. Values of $D_{dis,cal}$ were 365, 533, and 921 nm for samples P1, P3, and P5, respectively, in reasonable agreement with the CLSM values.

The values of D_{dis} are plotted in Figure 1 to be compared with the hydrodynamic diameters D_h. There is a strong correlation between D_{dis} and D_h such that D_{dis} is consistently (about 10−20%) larger than D_h. This suggests that the crystalline structure at the melting point is not a perfectly close-packed state of equivalent spheres of diameter D_h, but there is a significant space between particles in the crystal, as in hard crystals. The volume fraction of an ideal hard-sphere system at the perfectly closed-packed state relative to that at the melting point is 0.74/0.545, whose cubic root s_c (=1.11) will measure the one-dimensional free space in the hard system. If we multiply D_h by this factor s_c, we have values rather close to D_{dis} (see the square symbols in Figure 1). This means that insofar as the crystallization concentrations are concerned, the present systems are crudely (but not exactly) describable as hard systems with particle diameter D_h.

However, this does not necessarily mean that their crystal structure is the same as that of hard systems. The present systems should be distinguished from hard systems with respect to interparticle potentials, as was already suggested by the dependence of the brush layer thickness on graft chain length. Namely, when the graft chains are short, they have a highly stretched conformation forming a CPB layer, and the interparticle potential between CPB-afforded particles would be rather "hard", since CPB layers dislike mixing with each other primarily for a conformational entropic reason.[21,34] However, as the graft chain length increases, the local conformation of graft chains near the outer surface of the brush layer would become more like that of a random coil, and thus the interparticle potential would become "softer". This would be reflected on crystal structure, not only on lattice dimension but on lattice structure itself.

The 2-D hcp planes ((001) planes) only exist in crystals featuring face-centered cubic (fcc), hexagonal close-packed (hcp), or random hexagonal close-packed (rhcp) structure. In the previous paper,[19] we reported that a SiP−PMMA hybrid particle (sample P3 in this paper) had a fcc structure. This result was obtained by observing the relative stacking mode of three successive (001) layers by the reflection mode of CLSM (see ref 19 for details). We carried out the same analysis here for more quantitative results. For samples P3 and P5, we succeeded in collecting 37 and 26, respectively, of independent sets of three-layer data by observing different positions in the crystals.

For sample P3, 35 out of the 37 sets of data indicated an fcc structure, while the remaining two sets indicated a hcp structure, meaning that the crystal of this sample is not purely of fcc type but a mixture of fcc and hcp lattices. (In this regard, the statement for this sample given in the previous paper that "the crystal had a fcc structure" should be accordingly corrected.) For sample P5, no hcp stacking was found, all of the 26 sets of data indicating fcc. We then attempted to make a similar analysis with sample P1, which had the shortest chain length. After many trials, we could get only three sets of stacking data with unequivocal information. (The resolution of reflection-mode CLSM is not high enough especially for small particle sizes and short interparticle distances.) While two sets of the sample P1 data were for fcc stacking, one was for hcp. These results suggest that the present systems generally include both hcp and fcc lattices with the population of hcp lattice probably increasing with decreasing chain length. This trend seems to be compatible with the mentioned expectation that the interparticle potential for shorter chain length would become more like that of hard systems, combined with the experimental fact that hard systems form crystals of rhcp type,[41−43] i.e., a random mixture of hcp and fcc.

Clearly, a more systematic and quantitative study using a more powerful experimental method is needed to comprehensively understand the chain length dependence of the colloidal crystal structure of CPB-afforded silica particles. We are currently carrying out a fluorescence-mode CLSM analysis with fluorescence-labeled hybrid samples with a larger core diameter and a wider range of graft chain lengths.[44]

Conclusions

A DLS study of monodisperse SiPs grafted with a CPB of PMMA in dilute acetone solution revealed that the hydrodynamic thickness h of the brush layer increased with increasing PMMA molecular weight with a large molecular weight exponent of 0.83. This was interpreted by a modified Daoud−Cotton-type scaling theory, disclosing the crossover chain length of the brush layer from CPB to SDPB regime. Irrespective of graft chain length, more concentrated suspensions of the hybrid particles showed a phase transition from a (disordered) fluid to a fully crystallized system with a narrow fluid/crystal coexisting regime. The critical concentration of crystallization decreased with increasing graft chain length, and the nearest-neighbor interparticle distance D_{dis} in the crystal approached to a micrometer scale as the graft molecular weight reached 500 000. Good correlation was observed between D_h and D_{dis} such that $D_{dis} = D_h \times (1.15 \pm 0.05)$. CLSM analysis suggested that the colloidal crystal is generally composed of both hcp and fcc lattices with the fraction of hcp lattice likely to increase with decreasing chain length.

Acknowledgment. This work was supported in part by a Grant-in-Aid for Scientific Research (Grant-in-Aid 17002007 and 17685010) from the Ministry of Education, Culture, Sports, Science, and Technology, Japan, and by Industrial Technology Research Grant Program in 2004 from the New Energy and Industrial Technology Development Organization (NEDO) of Japan. We thank Nippon Shokubai Co. Ltd. for their kind donation of silica particle.

References and Notes

(1) Habdas, P.; Weeks, E. R. *Curr. Opin. Colloid Interface Sci.* **2002**, *7*, 196−203.
(2) Yethiraj, A.; van Blaaderen, A. *Nature (London)* **2003**, *421*, 513−517.
(3) Kegel, W. K.; van Blaaderen, A. *Science* **2000**, *287*, 290−293.
(4) Pusey, P. N.; van Megen, W. *Nature (London)* **1986**, *320*, 340−342.
(5) van Megen, W.; Underwood, S. M. *Nature (London)* **1993**, *362*, 616−618.
(6) Kose, A.; Hachisu, S. *J. Colloid Interface Sci.* **1974**, *46*, 460−469.
(7) Hachisu, S.; Kobayashi, Y.; Kose, A. *J. Colloid Interface Sci.* **1973**, *42*, 342−348.
(8) Hachisu, S.; Takano, K. *Adv. Colloid Interface Sci.* **1982**, *16*, 233−252.
(9) Cheng, Z.; Russel, W. B.; Chaikin, P. M. *Nature (London)* **1999**, *401*, 893−895.
(10) Zhu, J.; Li, M.; Rogers, R.; Meyer, W.; Ottewill, R. H.; STS-73 Space Shuttle Crew; Russel, W. B.; Chaikin, P. M. *Nature (London)* **1997**, *387*, 883−885.
(11) Auer, S.; Frenkel, D. *Nature (London)* **2001**, *409*, 1020−1023.
(12) Gasser, U.; Weeks, E. R.; Schofield, A.; Pusey, P. N.; Weitz, D. A. *Science* **2001**, *292*, 258−262.
(13) Gast, A. P.; Monovoukas, Y. *Nature (London)* **1991**, *351*, 553−555.
(14) Yablonovitch, E. *Nature (London)* **1999**, *401*, 539−541.
(15) Arsenault, A.; Fournier-Bidoz, S.; Hatton, B.; Míguez, H.; Tétreault, N.; Vekris, E.; Wong, S.; Yang, S. M.; Kieaev, V.; Ozin, G. A. *J. Mater. Chem.* **2004**, *14*, 781−794.
(16) Colvin, V. L. *MRS Bull.* **2001**, *26*, 637−641.
(17) Hiltner, P. A.; Krieger, I. M. *J. Phys. Chem.* **1969**, *73*, 2386−2389.
(18) Okubo, T. *Prog. Polym. Sci.* **1993**, *18*, 481−517.
(19) Ohno, K.; Morinaga, T.; Takeno, S.; Tsujii, Y.; Fukuda, T. *Macromolecules* **2006**, *39*, 1245−1249.
(20) Tsujii, Y.; Ohno, K.; Yamamoto, S.; Goto, A.; Fukuda, T. *Adv. Polym. Sci.* **2006**, *197*, 1−45.
(21) Fukuda, T.; Tsujii, Y.; Ohno, K. In *Macromolecular Engineering. Precise Synthesis, Materials Properties, Applications*; Matjaszewski, K., Gnanou, Y., Leibler, L., Eds.; Wiley-VCH: Weinheim, Germany, 2007; pp 1137−1178.
(22) Alexander, S. *J. Phys. (Paris)* **1977**, *38*, 983−987.
(23) (a) de Gennes, P. G. *J. Phys.*(*Paris*) **1976**, *37*, 1445−1452. (b) de Gennes, P. G. *Macromolecules* **1980**, *13*, 1069−1075.
(24) Milner, S.T.; Witten, T. A.; Cates, M. E. *Macromolecules* **1988**, *21*, 2610−2619.
(25) Lai, P.-Y.; Haperin, A. *Macromolecules* **1991**, *24*, 4981−4982.
(26) Daoud, M.; Cotton, J. P. *J. Phys. (Paris)* **1982**, *43*, 531−538.
(27) Birstein, T. M.; Zhulina, E. B. *Polymer* **1984**, *25*, 1453−1461.
(28) Dan, N.; Tirrell, M. *Macromolecules* **1992**, *25*, 2890−2895.
(29) (a) Wijmans, C. M.; Zhulina, E. B. *Macromolecules* **1993**, *26*, 7214−7224. (b) Li, H.; Witten, T. A. *Macromolecules* **1994**, *27*, 449−457. (c) Lin, E. K.; Gast, A. P. *Macromolecules* **1996**, *29*, 390−397.
(30) Yamamoto, S.; Tsujii, Y.; Fukuda, T. *Macromolecules* **2000**, *33*, 5995−5998.
(31) Yamamoto, S.; Ejaz, M.; Tsujii, Y.; Matsumoto, M.; Fukuda, T. *Macromolecules* **2000**, *33*, 5602−5607.
(32) Yamamoto, S.; Ejaz., M.; Tsujii, Y.; Fukuda, T. *Macromolecules* **2000**, *33*, 5608−5612.
(33) Urayama, K.; Yamamoto, S.; Tsujii, Y.; Fukuda, T.; Neher, D. *Macromolecules* **2002**, *35*, 9459−9465.
(34) (a) Yoshikawa, C.; Goto, A.; Tsujii, Y.; Fukuda, T.; Kimura, T.; Yamamoto, K.; Kishida, A. *Macromolecules* **2006**, *39*, 2284−2290. (b) Yoshikawa, C.; Goto, A.; Tsujii, Y.; Ishizuka, N.; Nakanishi, K.; Fukuda, T. *J. Polym. Sci., Part A: Polym. Chem.* **2007**, in press.
(35) (a) Ejaz, M.; Yamamoto, S.; Ohno, K.; Tsujii, Y.; Fukuda, T. Macromolecules **1998**, *31*, 5934−5936. (b) Husseman, M.; Malmström, E. E.; McNamara, M.; Mate, M.; Mecerreyes, D.; Benoit, D. G.; Hedrick, J. L.; Mansky, P.; Huang, E.; Russell, T. P.; Hawker, C. J.; Macromolecules **1999**, *32*, 1424−1431. (c) Matyjaszewski, K.; Miller, P. J.; Shukla, N.; Immaraporn, B.; Gelman, A.; Luokala, B. B.; Siclovan, T. M.; Kickelbick, G.; Vallant, T.; Hoffmann, H.; Pakula, T. *Macromolecules* **1999**, *32*, 8716−8724. (d) Jeyaprakash, J. D.; Samuel, S.; Dhamodharan, R.; Rühe, J. *Macromol. Rapid Commun.* **2002**, *23*, 277−281. (e) Mori, H.; Boker, A.; Krausch, G.; Müller, A. H. E. *Macromolecules* **2001**, *34*, 6871−6882. (f) Kim, J.-B.; Bruening, M. L.; Baker, G. L. *J. Am. Chem. Soc.* **2000**, *122*, 7616−7617. (g) Sedjo, R. A.; Mirous, B. K.; Brittain, W. J. *Macromolecules* **2000**, *33*, 1492−1493. (h) von Werne, T.; Patten, T. E. *J. Am. Chem. Soc.* **1999**, *121*, 7409−7410. (i) Perruchot, C.; Khan, M. A.; Kamitsi, A.; Armes, S. P.; von Werne, T.; Patten, T. E. *Langmuir* **2001**, *17*, 4479−4481. (j) Huang, X.; Wirth, M. J. *Anal. Chem.* **1997**, *69*, 4577−4580. (k) Jones, D. M.; Brown, A. A.; Huck, W. T. S. *Langmuir* **2002**, *18*, 1265−1269.
(36) Ohno, K.; Morinaga, T.; Koh, K.; Tsujii, Y.; Fukuda, T. *Macromolecules* **2005**, *38*, 2137−2142.
(37) Ohno, K.; Koh, K.; Tsujii, Y.; Fukuda, T. *Angew. Chem., Int. Ed.* **2003**, *42*, 2751−2754.
(38) Savin, D. A.; Pyun, J.; Patterson, G. D.; Kowalewski, T.; Matyjaszewski, K. *J. Polym. Sci., Part B: Polym. Phys.* **2002**, *40*, 2667−2676.

(39) Hoover, W. G.; Ree, F. H. *J. Chem. Phys.* **1968**, *49*, 3609−3617.
(40) Alder, B. J.; Hoover, W. G.; Young, D. A. *J. Chem. Phys.* **1968**, *49*, 3688−3696.
(41) Pusey, P. N., van Megen, W.; Bartlett, P.; Ackerson, B. J. *Phys. Rev. Lett.* **1989**, *63*, 2753−2756.
(42) Verhaegh, N. A. M.; van Duijneveldt, J. S.; van Blaaderen, A.; Lekkerkerker, H. N. W. *J. Chem. Phys.* **1995**, *102*, 1416−1421.
(43) (a) Elliot, M. S.; Bristol, B. T. F.; Poon, W. C. K. *Physica A* **1997**, *235*, 216−223. (b) Elliot, M. S.; Poon, W. C. K. *Adv. Colloid Interface Sci.* **2001**, *92*, 133−194.
(44) Morinaga, T.; et al. To be published.
(45) Ma, Y. D.; Fukuda, T.; Inagaki, H. *Polym. J.* **1983**, *15*, 673−681.

MA071770Z